Investigation of Thermophysical Properties of $CuFeS_2$ Nanoparticles Prepared by Pulsed Laser Ablation Technique.

R. Onsi [a*], ***M. Nabil*** [a], ***k. Easawi*** [a], ***S. Abdallah*** [a] ***and S. Negm*** [a]

[a] *Basic Engineering Sciences department, Faculty of Engineering, Benha University, Egypt*

In this study, we used the pulsed laser ablation technique in liquid (PLAL) with varying ablation times to successfully synthesize copper iron sulfide ($CuFeS_2$) nanoparticles (NPs) in different sizes. Transmission electron microscopy (TEM) data reveals that $CuFeS_2$ NPs exhibit a spherical structure, with an average size of 17.9, 35.2, and 44.2 nm for ablation times of 15, 30, and 45 minutes, respectively. We employed mapping and energy disperse x-ray (EDX) to display the distribution and percentage of each element in the sample.The bonds between elements were confirmed using Fourier transform infrared (FTIR) studies. The molecular structure as well as the molecule's geometry and even symmetry can be determined using Raman spectroscopy. According to the UV-Vis spectrum, the absorption peaks of $CuFeS_2$ NPs move to the right as the ablation time increases. As the particle size was grown, the associated band gap energy dropped from 2.68 eV to 2.11 eV. We developed a photoacoustic method (PA) to evaluate the thermophysical parameters of $CuFeS_2$ nanofluid. Thermal effusivity (**e**), thermal diffusivity (**α**), and thermal conductivity (**k**) were obtained for the different samples using the closed-cell PA technique. The thermal conductivity of the samples increases from 0.636 to 0.9623 W/mK with the increase in the particle size from 17.9 nm to 44.2 nm.

Keywords

Copper iron sulfide, Laser ablation, Photoacoustic technique, Thermal conductivity

Corresponding Author: romany.eed@feng.bu.edu.eg

Receive Date: 29-9-2024; Revise Date: 18-10-20242024; Accept Date: 25-10-2024; Publish: 25-10-2024

1. Introduction

Transition metal oxides (TMOs) have received attention due to their special characteristics, but they have low electrical conductivity. Thus, scientists attempt to investigate alternative electrode materials that may possess the essential qualities of a desirable electrode material, such as stability, environmental friendliness, and electrical conductivity. Transition metal sulfides (TMSs) have piqued the interest of researchers due to their ability to effectively replace oxygen in compounds, resulting in compounds with enhanced ionic diffusivity. In addition to having a higher electrical conductivity than oxides, sulfides are less expensive and have superior electrochemical performance [1]. $CuFeS_2$ is a tetragonal element belonging to the I-III-VI family of elements [2, 3]. Researchers want to study them since they are abundant in nature and have little toxicity. $CuFeS_2$ is a typical n-type semiconductor, and it has a quite narrow bandgap. $CuFeS_2$ exhibits superior photoelectric and magnetic properties, making it a favorable material for solar cells. Researchers have published numerous studies on the synthesis of $CuFeS_2$ using various solutions, such as hydrothermal, chemical bath, solvothermal hot injection, and one-pot methods. $CuFeS_2$/graphene composite electrode manufacturing is complex and requires binder, which raises costs and decreases performance.

The creation of NPs using **PLAL** has drawn a lot of interest as a novel method of producing them. Their unique physical characteristics, along with their severe Plasmonic absorption peak at the visible area, make them highly desirable for biochemical, biophysical, and biotechnological applications. This technique involves focusing a laser beam on a large target and ablating the material surface. A delayed mass expands beneath the liquid, releasing a variety of species, among them NPs. A liquid environment surrounds the ablated plume, creating NPs through sudden molten bubble condensation, collisions between plume species, or the nucleation of clusters from free atoms [4]. The three main benefits of using the **PLAL** method to manufacture nanoparticles are their high stability, relative ease of preparation, and lack of chemical reagents in the final product [5]. Consequently, we produced $CuFeS_2$ nanoparticles in ethanol using the laser ablation technique [6]. Recently, there has been a lot of interest in the thermophysical characteristics of nanofluids, such as thermal effusivity (**e**), thermal diffusivity (**α**), and thermal conductivity (**K**). Relationships (1) and (2) establish the relations between diffusivity, effusivity, conductivity, and volumetric-specific heat $\mathbf{c_p}$ [8].

$$\alpha = \frac{K}{\rho\, C_p} \qquad (1)$$

$$e = \sqrt{K\, \rho\, C_p} \qquad (2)$$

where $\mathbf{c_p}$ is the molar-specific heat at constant pressure and **ρ** is the sample's density. The ability of the sample to interchange heat with the environment is measured by thermal effusivity (**e**), and the effectiveness of heat diffusion through the sample is measured by

thermal diffusivity (**α**), a crucial thermophysical parameter [7]. Given **e** and **α**, the sample conductivity **k** may be calculated using equation (3).

$$K = e\sqrt{\alpha} \qquad (3)$$

Using procedures for non-radiative de-excitation that come after optical absorption, the PA approach is a photothermal detection technique that has proven to be an effective tool for examining the optical and thermal properties of the materials. In addition to being noncontact and nondestructive, the PA method has gained popularity due to its elegant, straightforward experimental design and its flexibility in using various arrangements to accurately measure the necessary thermophysical parameters. We present the PA method as a useful, non-intrusive way to find out about the thermal properties of very small amounts of nanoparticles NPs in liquids that don't absorb them [8].

In this work, we successfully synthesize different sizes of $CuFeS_2$ NPs in ethanol using the pulsed laser ablation technique. TEM, EDX, FTIR, and Raman spectroscopy were measured to analyze the obtained samples. Using the photoacoustic method, the diffusivity (**α**), effusivity (**e**), and conductivity (**k**) were measured.

2. Experimental

2.1. Materials and methods.

The alloy target, which included sulfur, copper, and iron, was bought from Sammlung Von, and ethanol was bought from Sigma Aldrich. Fig. 1 depicts the experimental setup schematically. A lens with a focal length of 20 cm focused the beam of a pulsed Q-Switched Nd:YAG laser with a pulse duration of 8 ns, a wavelength of 1064 nm, and a repetition rate of 10 Hz on the target's surface (purity: 99.999% from Sigma Aldrich). The target was put at the bottom of a glass container holding 20 milliliters (ml) of ethanol (Sigma Aldrich) and had dimensions of 2 by 2 centimeters. The target was mounted at 16 mm below the liquid surface after being cleaned for 30 minutes with ethanol and distilled water to remove organic contaminants. The target was first cleaned using the ultrasonic bath. The ablation time ranged from 15 minutes to 45 minutes, using a laser power of 480 mj. The liquid was initially colorless, but it soon started to turn yellow and eventually brown. Based on a UV-Vis absorption spectrum, the browner color of the solutions indicates a larger concentration of $CuFeS_2$ NPs. When the laser beam strikes a material, its surface transmits the energy it carries to the highest layers of the substance. The result is a temperature rise that is higher than the melting point. Surface melting, vaporization, and material ejection result from the extreme power being given in only some millisecond pulses because the energy density surpasses the material's ablation threshold. Different species, including ions, molecules, and particles, are released from the surface during this process, absorbing received energy to create plasma [9–12].

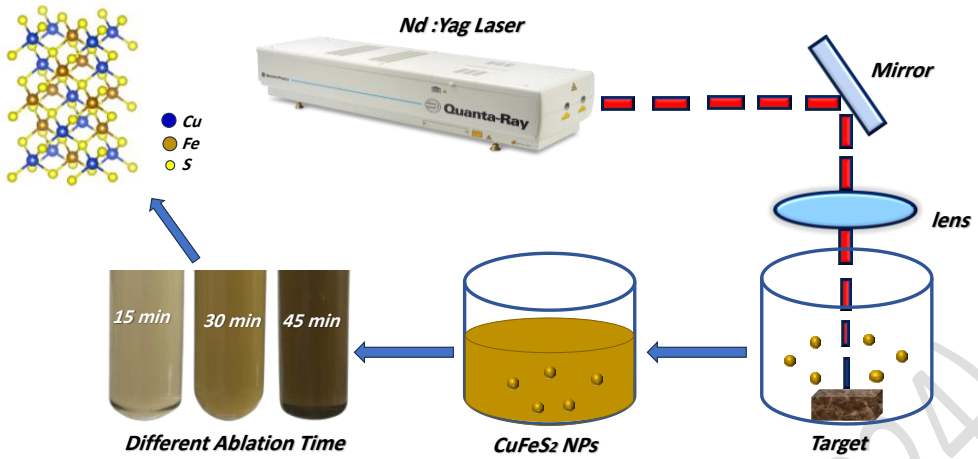

Fig. 1: Pulsed Laser Ablation Technique.

When the process occurs in a liquid, the temperature of the plasma plume rapidly drops and spherical nanoparticles are formed.

2.1. Instrumentation

A lens with a focal length of 20 cm was employed to concentrate a 1064 nm wavelength, 8 ns pulse duration, and 10 Hz repetition rate Nd: YAG (Quanta-Ray) laser on the target's surface. The (COHERENT-LASERMATE/D) power meter was used to measure the incident laser pulse's energy. Immediately following the ablation operation, the $CuFeS_2$ nanoparticles' absorption spectra in ethanol were examined via a UV-Vis double-beam spectrometer of the JASCO V-670 type. Using an HRTEM (JEM-2100), the nanoparticles' size distribution and form were ascertained. $CuFeS_2$ nanocomposite's functional group organization is determined using FTIR (Bruker ALPHA IA, Germany) and Raman Spectra (HORIBA-LABRAM HR EVO) in the 4000–400 cm^{-1} range. To comprehend the $CuFeS_2$ sample's surface shape and elemental structure, EDX analysis and the TEM (JEOL JEM-2010 F) were used. The MTEC Model 300, a highly sensitive (PA), was employed to ascertain the thermal characteristics of $CuFeS_2$ samples.

3. Results and discussion.

3.1. TEM Analysis

As seen in **Fig. 2**, the general microstructures of the $CuFeS_2$ samples were examined using HR-TEM (JEM-2100) analysis. The creation of spherical $CuFeS_2$ nanoparticles is confirmed by the TEM images. The two-dimensional (2D) spherical nanoparticles' shape can propose a huge surface area and improved electrochemical energy storage capabilities. As a result, these materials are thought to be interesting candidates for use in supercapacitors due to their enormous surface area **[13]**. **Fig. 2 (a, b, c)** displays the size distribution and TEM micrograph of samples of $CuFeS_2$ NPs produced by a pulsed laser for ablation times of 15, 30, and 45 minutes in an ethanol solution at a laser intensity of

480 mJ. After a 15-minute ablation period, the generated NPs' estimated average size was 17.9 nm; however, when the ablation duration was extended to 30 and 45 minutes, the size grew to 35.2 nm and 44.2 nm, respectively. The interaction of the generated nanoparticles with the laser light for longer periods of ablation was the cause of this rise in particle size. The small particles squeeze and merge into larger particles when they come into contact with one another by increasing the ablation time [14].

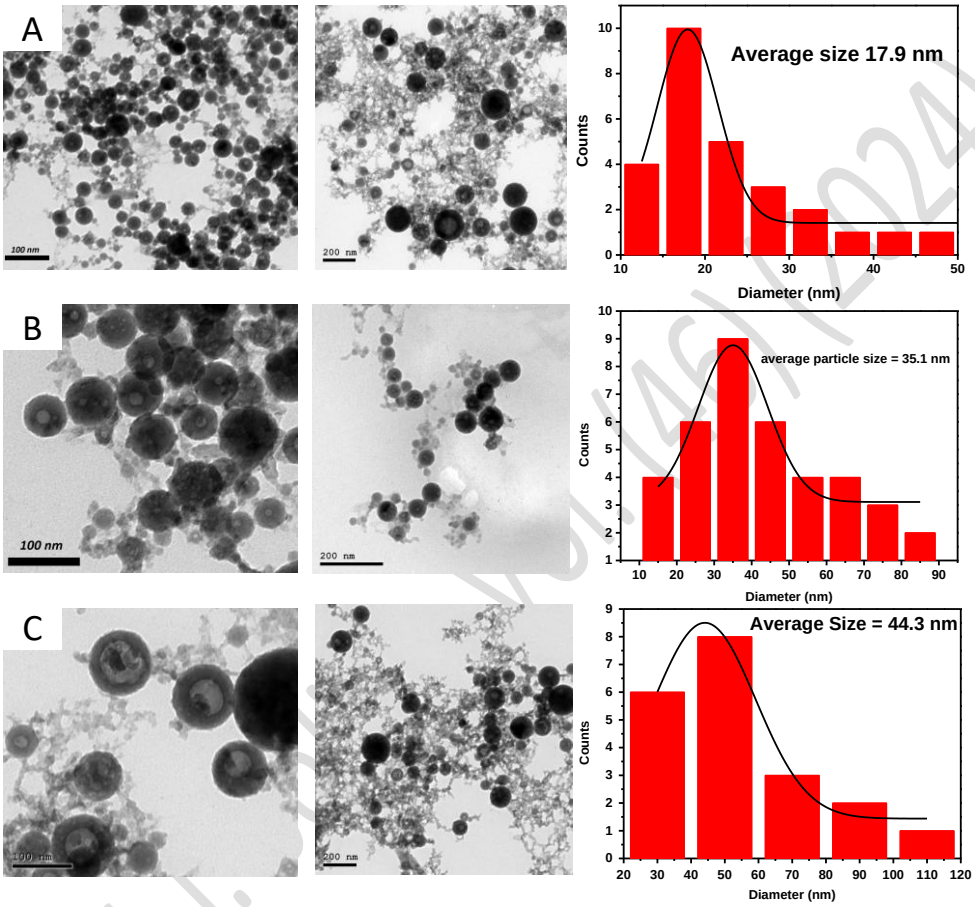

Fig. 2. TEM images of $CuFeS_2$ nanoparticles (a) 15 minutes ablation time; (b) 30 minutes ablation time; (c) 45 minutes ablation time.

Consequently, larger particles are formed at longer ablation periods, and the narrower particle distribution indicates that no significant aggregation is observed.`

3.2 EDX and Mapping Analysis

The EDX results for the acquired samples are shown in Fig. 3. The results confirm the purity of the samples and the ratio of elements produced in each sample. Additionally, Fig. 4 illustrates the elemental distribution, TEM characterization, and matching elemental mapping of $CuFeS_2$ nanoparticles.

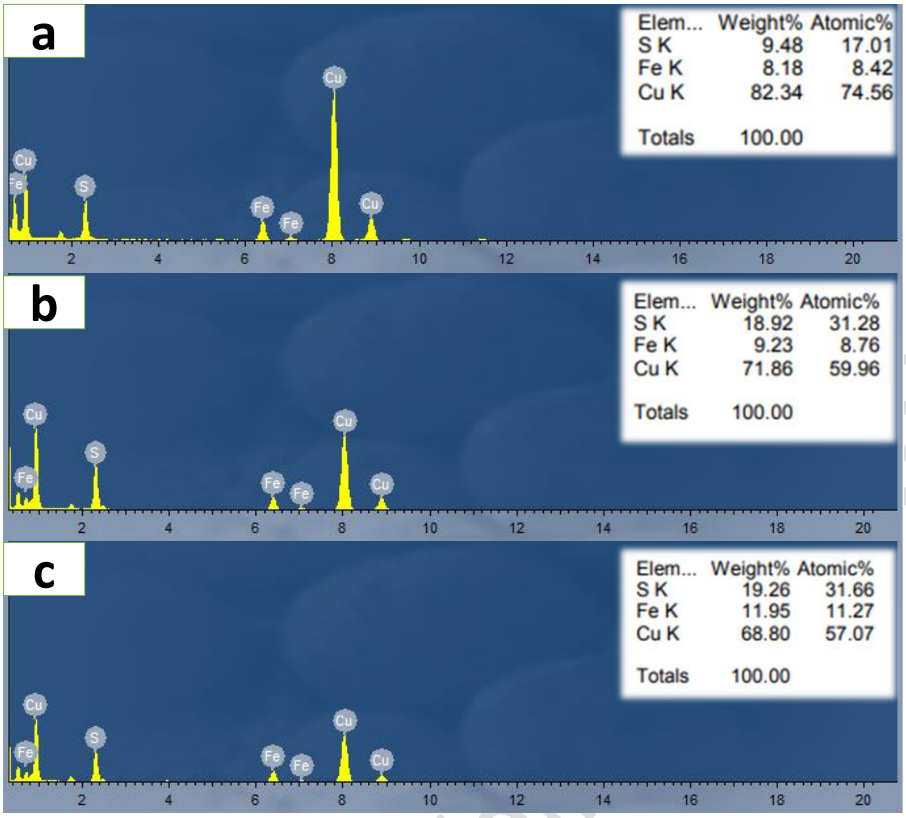

Fig. 3. EDX for $CuFeS_2$ (a) 15 minutes of ablation time, (b) 30 minutes of ablation time, and (c) 45 minutes of ablation time.

With EDX mapping, the elemental compositions of the resulting samples (Cu, S, and Fe) are determined and an atomically consistent distribution is displayed.

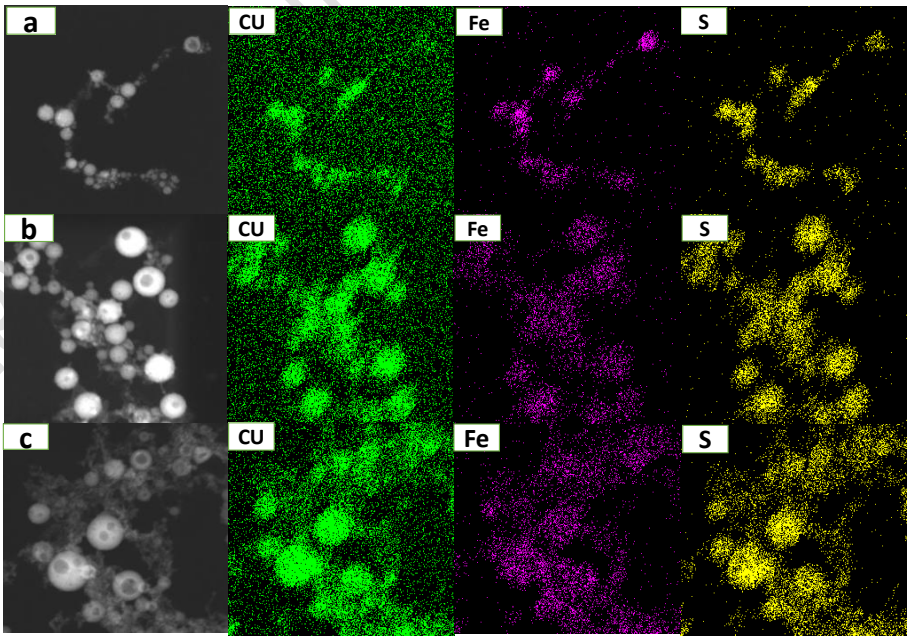

Fig. 4. EDX and Mapping for (a) 15 minutes (b) 30 minutes (c) 45 minutes

By using a laser ablation approach, the elemental mapping verifies that Fe, Cu, and S are present in the three samples of $CuFeS_2$.

3.3. FTIR Measurements

FTIR spectroscopy is a useful tool for learning more about the structure of products and how raw materials react. **Fig. 5** shows Ftir measurement for $CuFeS_2$ NPs sample with ablation time 30 minutes and laser energy 480 mj. Three peaks can be seen in **Fig. 5** for $CuFeS_2$ NPs, which are corresponding to the O-H bending vibration and the C=S stretching vibration, in that order, at 1043, 1639, and 3265 cm^{-1}. The observed O-H bending in the produced $CuFeS_2$ nanoparticles is attributed to the preparation of the $CuFeS_2$ NPs in ethanol, which is known to contain O-H groups.

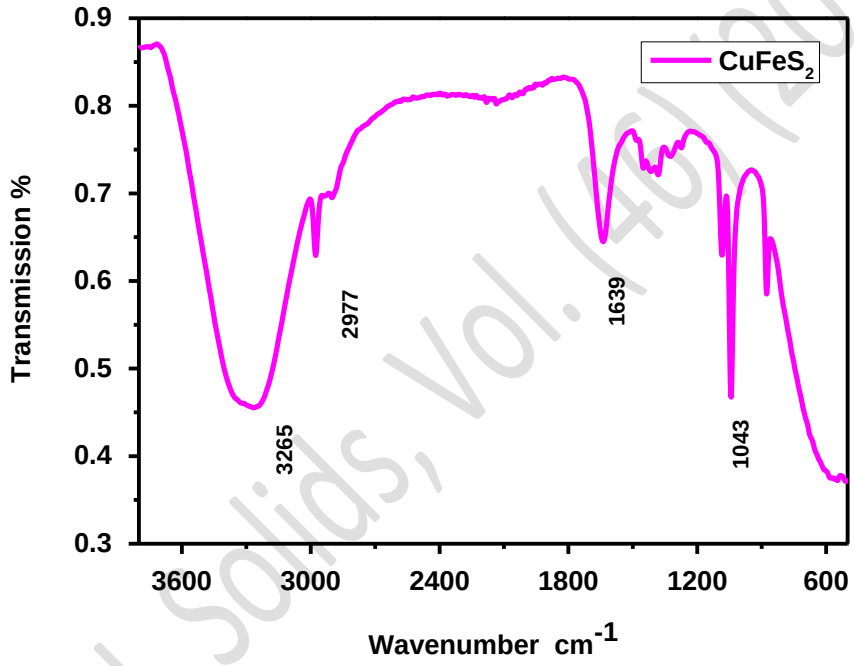

Fig. 5. FTIR for $CuFeS_2$ nanoparticles at 30 min ablation time.

The L-cysteine precursor may be responsible for the C=S stretching in the produced $CuFeS_2$ **[15]**.

3.4. Raman Spectroscopy

The molecular structure can be ascertained via Raman spectroscopy, as can the geometry and even symmetry of the molecule. **Fig. 6** displays Raman spectra for the $CuFeS_2$ NPs sample at ablation time 30 minutes. It displays peaks at wavenumbers of 216, 275, 385, 473, and 580 cm^{-1}, ranging from 200 to 700 cm^{-1}. Cu-S and Fe-S bonds are represented by the distinctive peaks of $CuFeS_2$ at 275, 473, and 385 cm^{-1}, respectively [16]. But in these circumstances, a peak linked to sulfur (216 cm^{-1}) is also more noticeable. The layers of chalcopyrite are composed of covalently bonded sulfur dimers between layers and solitary sulfur atoms within layers. It is interesting to notice that the peaks at the Raman

spectra, which correspond to the S-S stretching band and lattice vibration, are 275 and 473 cm^{-1}.

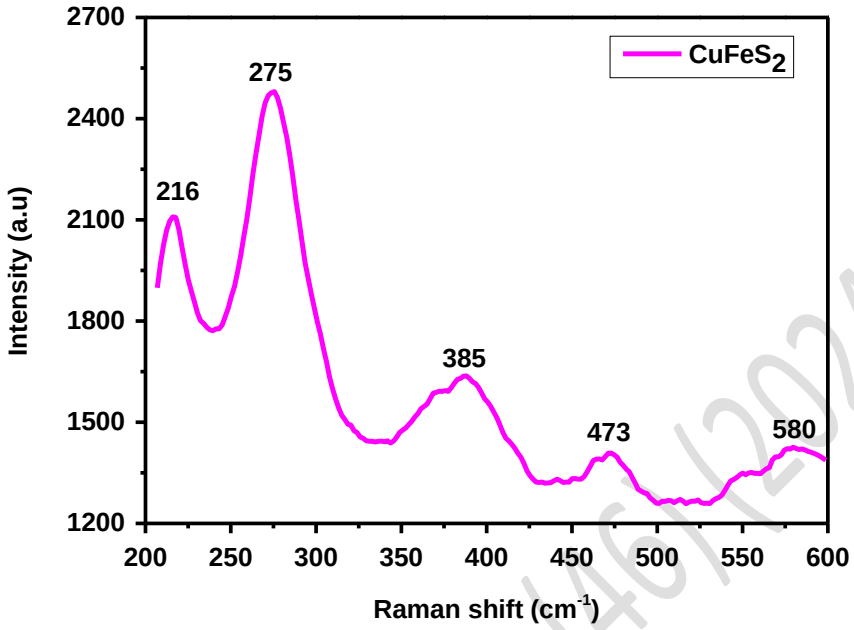

Fig. 6. Raman Spectroscopy for $CuFeS_2$ nanoparticles at 30 min ablation time.

Additionally, corresponding to the data stated, the three peaks, such as 275, 385, and 473 cm^{-1} are the characteristic peaks of $CuFeS_2$ [13].

3.5. Optical Characterization

The $CuFeS_2$ nanoparticles that were produced at varying ablation times had their absorption spectra analyzed. Fig. 7 illustrates a red shift in wavelength with increasing ablation time, indicating an increase in $CuFeS_2$ nanoparticle particle size, which is explained by the quantum confinement effect.The rise in concentration and volume fraction of $CuFeS_2$ nanoparticles within the liquid is the cause of the increased peak intensity of the spectra. The key element in optical absorption is electronic transitions. Tauc's equation can be used to express the selection principles that govern these transitions:

$$\alpha h\upsilon = A\,(h\upsilon - E_g)^m \qquad (4)$$

where **m** is a constant, **A** is a constant, **hυ** is the incident photon energy, and **α** is the absorption coefficient. For direct and indirect transitions, respectively, permissible values of m are (1/2 and 2), while not allowed values are (3/2 and 3).

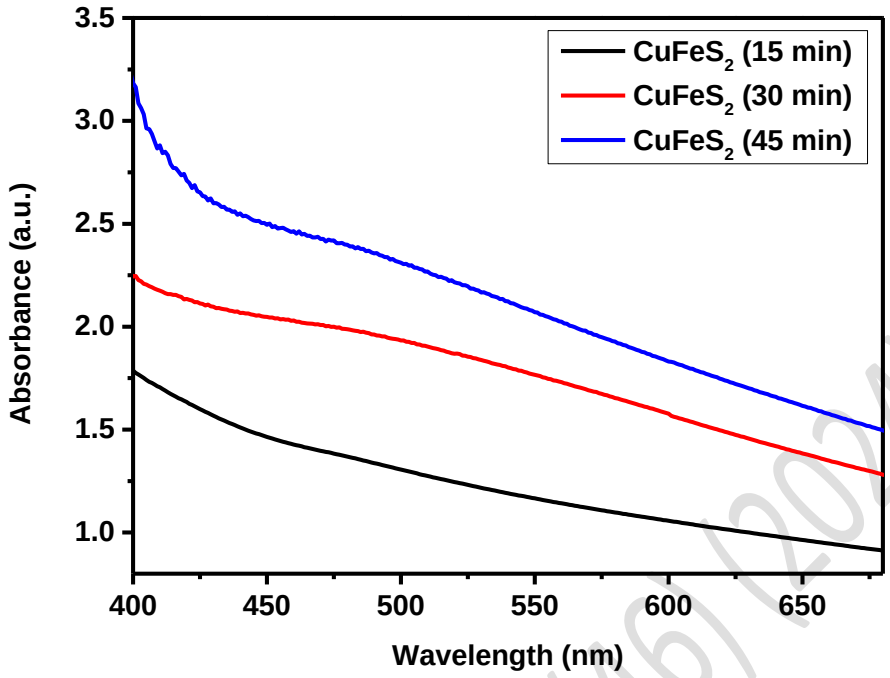

Fig. 7. UV absorption spectra for $CuFeS_2$ nanoparticles prepared at different ablation times.

As can be observed in **Fig. 8**, the real value of the band gap is found using the Tauc-plot curve of $(\alpha h\upsilon)^2$ values against $(h\upsilon)$.

Ablation Time (min)	Particle Size (nm)	Band Gap Energy (ev)
15	17.9	2.68
30	35.2	2.47
45	44.2	2.11

Table 1: particle size and bandgap energy for different ablation times.

The bandgap values of $CuFeS_2$ NPs in ethanol were determined from the energy axis's intercept via the Tauc-plot calculation. The estimated bandgap values are given in **Table 1**. The optical bandgap reduces as $CuFeS_2$ NP size grows in ethanol and vice versa, as seen by **Fig. 8** and **Table 1**. Put otherwise, the absorption edge moves near smaller bandgap values as particle size rises, from 2.68 eV (17.9 nm) to 2.11 eV (44.2 nm).

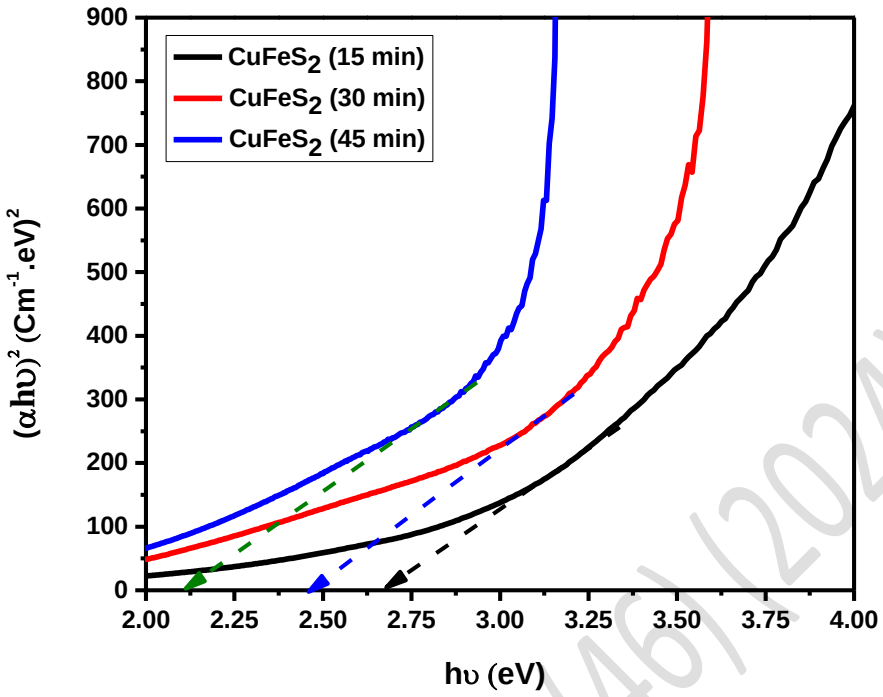

Fig. 8. Band gap energy for samples prepared at different ablation times.

This is ascribed to the impact of the quantum confinement effect. Thus, for suitable opto-electronic applications, the bandgap of such materials can be tuned [17].

3.6. Thermal Characterization

The basic principle of the PA approach is as follows: the prepared sample is put in a sealed compartment that is occupied with air, and it is exposed to monochromatic light of any wavelength that is required, with intensity controlled at an appropriate acoustic frequency (**f**), as illustrated in Fig. 9. The nonradiative decaying of the absorbed radiation causes heat to periodically escape the sample into the air near its surface. An acoustic signal is produced by this temperature differential in the cell's air, and a sensitive microphone mounted to the chamber detects this sound [8].

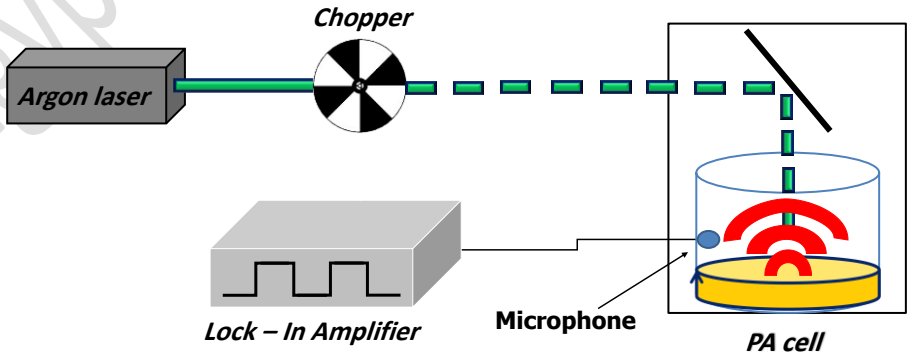

Fig. 9. Photoacoustic Technique

Since we used Poult and Chambron's [8] analysis for thermally thick samples in this work, the PA amplitude (**q**) and phase (∅) are provided by:

$$q = \frac{A\beta\mu_s}{2\pi f e\sqrt{(\beta\mu_s+1)^2+1}} \qquad (5)$$

$$\tan\emptyset = \beta\mu_s + 1 \qquad (6)$$

where **e** is the sample effusivity and **β** (1/μs) is the coefficient of optical absorption, **A** is a constant (unrelated to the sample) and can be expressed as follows:

$$A = \frac{\gamma P_o I_O \alpha_g^{1/2}}{2 l_g T_o} \qquad (7)$$

where $\mathbf{T_0}$ and $\mathbf{P_0}$ are the ambient temperature and pressure, $\mathbf{I_0}$ is the incidence intensity, $\mathbf{L_g}$ is the cell's internal gas column's length, and $\boldsymbol{\alpha_g}$ is the gas's diffusivity. It is evident that calculating the thermal characteristics of thermally thick samples with knowing **β** is straightforward and simple when using formulas (5) and (6). It is evident that whereas (**e**) can be calculated using amplitude measurements, (α) can only be detected using phase measurements (Eq. 6).In order to calculate (**e**) using Eq. (5), nonrelated sample constant **A** must be removed [8]. Normalization with a reference sample of known thermal properties might be used to accomplish this. As a result, dividing $\mathbf{q_r}$ of a reference sample by **q** of an NFs sample yields the inverse normalized amplitude (q_n^{-1}). If the **β** of the reference sample is the same, (q_n^{-1}) can be calculated as follows:

$$q_n^{-1} = \frac{q_r}{q} = \frac{e\,\alpha_r^{1/2}}{e_r\alpha^{1/2}}\sqrt{\frac{(\beta\sqrt{\alpha/\pi f}+1)^2+1}{(\beta\sqrt{\alpha_r/\pi f}+1)^2+1}} \qquad (8)$$

According to Eq. (8), (**e**) can be determined by knowing both of **α** and **β** as well as the reference sample's thermal characteristics ($\mathbf{e_r}$ and $\boldsymbol{\alpha_r}$) [8]. The current concern is how the thermal characteristics of non-absorbing liquids may be measured using the PA method, which uses optical absorption as a means of producing heat. We propose using a dye agent at a concentration that does not alter the thermal characteristics of the liquids to resolve this discrepancy. Because light absorption within the sample enables the formation of the PA signal in this manner, the effective transparency of the samples required by the open PA cell methodology is not required in this case. Thus, this technique may be used to measure the thermal characteristics of both high- and low-volume concentration nanofluids. The relation of (**q**) versus (**f**) is displayed in Fig. 10 (a, b, c, and d) for pure ethanol and $CuFeS_2$ nanoparticles in ethanol of sizes 17.9, 34.9, and 44.3 nm, respectively. The effusivity (**e**) and diffusivity (**α**) can be obtained for each sample from Fig. 10 by using the best fitting. So, the thermal conductivity (**k**) can be calculated by giving the equation:

$$k = e\sqrt{\alpha} \qquad (9)$$

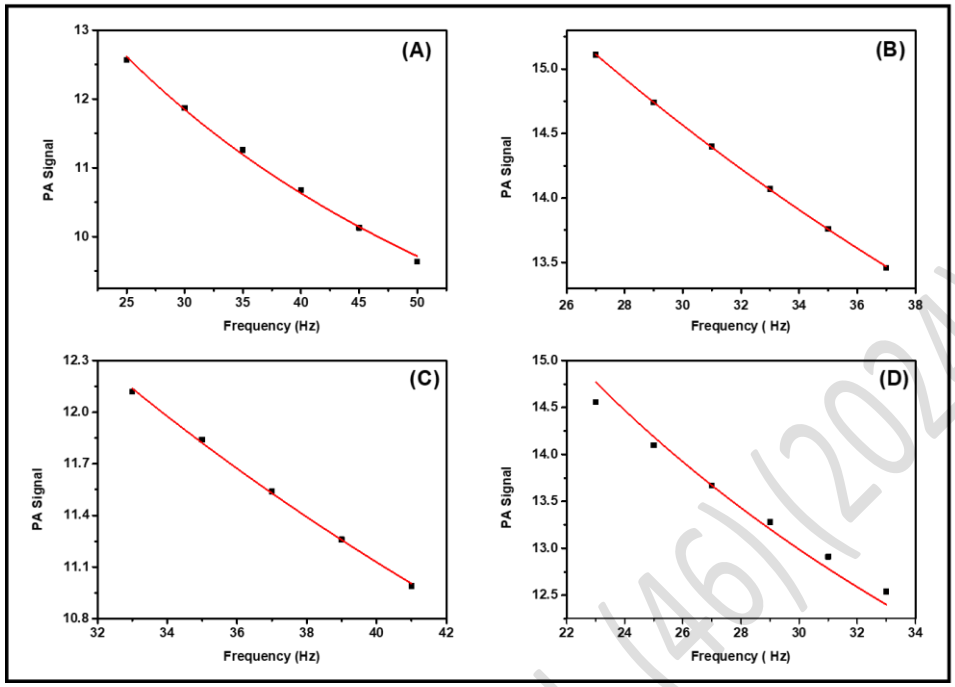

Fig. 10. PA Signal Vs Chopper Frequency for (A) Pure Ethanol, (B) $CuFeS_2$ sample at 15 min, (C) $CuFeS_2$ sample at 30 min, and (D) $CuFeS_2$ at 45 min.

It was observed from **Table (2)** that, in the case of $CuFeS_2$ nanoparticles in ethanol, the thermal conductivity improves from 0.17 W/m·K in pure ethanol to 0.9623 W/m·K in the presence of $CuFeS_2$ nanoparticles. This increase in conductivity (**K**) was caused by the presence of $CuFeS_2$ NPs.

	Average particle size (nm)	Diffusivity (m^2/s)	Effusivity ($ws^{1/2}m^{-2}k^{-1}$)	Conductivity ($w\ m^{-1}k^{-1}$)
Pure ethanol	--	$8.9*10^{-8}$	569.841	0.17
15 min sample	17.9	2.658	0.39045	0.636
30 min sample	35.2	3.256	0.44775	0.8079
45 min sample	44.3	3.467	0.51682	0.9623

Table 2: Thermal effusivity, thermal diffusivity, and thermal conductivity for different samples

It was also observed from **Table (2)** that, when the $CuFeS_2$ nanoparticle size increases from 17.9 to 44.3 nm, the thermal conductivity increases from (0.636 to 0.9623) $w\ m^{-1}k^{-1}$. The reason for this is that as the size of the $CuFeS_2$ nanoparticles increases for the same concentration, the thermal conductivity (**K**) increases due to less scattering of the phonon at the boundary of the nanoparticles. The smaller sizes produce more scattering of the phonon than the largest size, resulting in less thermal conductivity **[22–27]**.

4.Conclusion

$CuFeS_2$ nanoparticles were prepared via the PLAL technique of a chalcopyrite target in ethanol, which served to prevent oxidation. The effect of ablation time was investigated using time durations of 15, 30, and 45 minutes under steady conditions (λ = 1064 nm, E = 480 mJ/pulse, in ethanol). The results showed that most nanoparticles across all samples are spherical and smaller than 100 nm, with a majority ranging between 17 and 50 nm. Longer durations of ablation times are probably less effective because of the primary nanoparticles' absorption of laser energy leading to particle fusion and an increase in average NP size to approximately 44 nm. The PA approach, a non-destructive, non-contact method, was used to test the thermal properties of $CuFeS_2$ nanofluids, including their diffusivity, effusivity, and conductivity. It was observed that thermal conductivity increased from 0.636 to 0.9623 $W \cdot m^{-1} \cdot K^{-1}$ with the growth in nanoparticle size.

Declaration of Conflicting Interests

The author(s) declared no potential conflicts of interest concerning the research, authorship, and/or publication of this article.

References

[1] B. Bhattacharyya and A. Pandey, "CuFeS2 Quantum Dots and Highly Luminescent CuFeS2 Based Core/Shell Structures: Synthesis, Tunability, and Photophysics," *J. Am. Chem. Soc.*, vol. 138, no. 32, pp. 10207–10213, 2016, doi: 10.1021/jacs.6b04981.

[2] S. Conejeros, P. Alemany, M. Llunell, I. D. P. R. Moreira, V. Sánchez, and J. Llanos, "Electronic Structure and Magnetic Properties of CuFeS2," *Inorg. Chem.*, vol. 54, no. 10, pp. 4840–4849, 2015, doi: 10.1021/acs.inorgchem.5b00399.

[3] W. Ding, X. Wang, H. Peng, and L. Hu, "Electrochemical performance of the chalcopyrite CuFeS 2 as cathode for lithium ion battery," *Mater. Chem. Phys.*, vol. 137, no. 3, pp. 872–876, 2013, doi: 10.1016/j.matchemphys.2012.09.072.

[4] R. Onsi, K. Easawi, S. Abdallah, S. Negm, and H. Talaat, "Preparation of Silver Nanoparticles Dispersed in Almond Oil Using Laser Ablation Technique," in *IOP Conference Series: Materials Science and Engineering*, 2020, vol. 762, no. 1. doi: 10.1088/1757-899X/762/1/012005.

[5] C. G. Moura *et al.*, "Effects of laser fluence and liquid media on preparation of small Ag nanoparticles by laser ablation in liquid," *Opt. Laser Technol.*, vol. 97, pp. 20–28, 2017, doi: 10.1016/j.optlastec.2017.06.007.

[6] H. Nsude et al., "Binder-free fabricated CuFeS 2 electrodes for supercapacitor applications," Mater. Res. Express, vol. 9, Feb. 2022, doi: 10.1088/2053-1591/ac4f13.

[7] M. I. Sarkar and K. Kumar, "Fabrication of photoacoustic cell and thermal diffusivity measurement of coal carbon black using it," *Mater. Today Proc.*, vol. 52, pp. 1812–1816, 2022, doi: 10.1016/j.matpr.2021.11.467.

[8] T. A. El-Brolossy and O. Saber, "Non-intrusive method for thermal properties measurement of nanofluids," *Exp. Therm. Fluid Sci.*, vol. 44, pp. 498–503, 2013, doi:

10.1016/j.expthermflusci.2012.08.011.

[9] M. Fernández-Arias *et al.*, "Palladium Nanoparticles Synthesized by Laser Ablation in Liquids for Antimicrobial Applications," *Nanomaterials*, vol. 12, no. 15, 2022, doi: 10.3390/nano12152621.

[10] E. Fazio *et al.*, "Nanoparticles engineering by pulsed laser ablation in liquids: Concepts and applications," *Nanomaterials*, vol. 10, no. 11, pp. 1–50, 2020, doi: 10.3390/nano10112317.

[11] H. Zeng *et al.*, "Nanomaterials via laser ablation/irradiation in liquid: A review," *Adv. Funct. Mater.*, vol. 22, no. 7, pp. 1333–1353, 2012, doi: 10.1002/adfm.201102295.

[12] T. Nishi, A. Takeichi, H. Azuma, N. Suzuki, T. Hioki, and T. Motohiro, "Fabrication of palladium nanoparticles by laser ablation in liquid," *J. Laser Micro Nanoeng.*, vol. 5, no. 3, pp. 192–196, 2010, doi: 10.2961/jlmn.2010.03.0002.

[13] P. Rupa Ranjani, P. M. Anjana, and R. B. Rakhi, "Solvothermal synthesis of CuFeS2 nanoflakes as a promising electrode material for supercapacitors," *J. Energy Storage*, vol. 33, no. August 2020, p. 102063, 2021, doi: 10.1016/j.est.2020.102063.

[14] Z. Huang *et al.*, " Manufacture of TiO 2 nanoparticles with high preparation efficiency and photocatalytic performance by controlling the parameters of pulsed laser ablation in liquid ," *Opt. Express*, vol. 30, no. 12, p. 20482, 2022, doi: 10.1364/oe.455658.

[15] H. Yu *et al.*, "Synthesis and characterization of CuFeS2 and Se doped CuFeS2−xSex nanoparticles," *J. Mater. Sci. Mater. Electron.*, vol. 30, no. 13, pp. 12269–12274, 2019, doi: 10.1007/s10854-019-01586-5.

[16] S. Sahoo, P. Pazhamalai, V. K. Mariappan, G. K. Veerasubramani, N. J. Kim, and S. J. Kim, "Hydrothermally synthesized chalcopyrite platelets as an electrode material for symmetric supercapacitors," *Inorg. Chem. Front.*, vol. 7, no. 7, pp. 1492–1502, 2020, doi: 10.1039/c9qi01335k.

[17] A. I. Abdel-salam, M. M. Awad, T. S. Soliman, and A. Khalid, "The effect of graphene on structure and optical properties of CdSe nanoparticles for optoelectronic application," *J. Alloys Compd.*, vol. 898, p. 162946, 2022, doi: 10.1016/j.jallcom.2021.162946.

[18] N. R. Dhineshbabu, V. Rajendran, N. Nithyavathy, and R. Vetumperumal, "Study of structural and optical properties of cupric oxide nanoparticles," *Appl. Nanosci.*, vol. 6, no. 6, pp. 933–939, 2016, doi: 10.1007/s13204-015-0499-2.

[19] A. S. Hassanien and A. A. Akl, "In fl uence of composition on optical and dispersion parameters of thermally evaporated non-crystalline Cd 50 S 50 À x Se x thin fi lms," vol. 648, pp. 280–290, 2015.

[20] T. S. Soliman, S. A. Vshivkov, and S. I. Elkalashy, "Structural , linear and nonlinear optical properties of Ni nanoparticles – Polyvinyl alcohol nanocomposite films for optoelectronic applications," *Opt. Mater. (Amst).*, vol. 107, no. April, p. 110037, 2020, doi: 10.1016/j.optmat.2020.110037.

[21] E. Koushki, S. H. Mousavi, S. A. Jafari Mohammadi, M. H. Majles Ara, and P. W. De Oliveira, "Optical properties of aluminum oxide thin films and colloidal nanostructures," *Thin Solid Films*, vol. 592, pp. 81–87, 2015, doi: 10.1016/j.tsf.2015.09.003.

[22] M. Goyal, "file:///E:/phd/dr romany/papers/romany papers/New paper1/Reference paper/thermal explanation.pdf," *Pramana - J. Phys.*, vol. 91, no. 6, pp. 1–5, 2018, doi:

10.1007/s12043-018-1660-8.

[23] E. V. Timofeeva, D. S. Smith, W. Yu, D. M. France, D. Singh, and J. L. Routbort, "Particle size and interfacial effects on thermo-physical and heat transfer characteristics of water-based α-SiC nanofluids," *Nanotechnology*, vol. 21, no. 21, 2010, doi: 10.1088/0957-4484/21/21/215703.

[24] Z. El-Qahtani, A. Badawi, K. Easawi, N. Al-Hosiny, and S. Abdallah, "Photoacoustic study of optical and thermal properties of alloyed CdTe xS1-x nanocrystals," Mater. Sci. Semicond. Process., vol. 20, no. 1, pp. 68–73, 2014, doi: 10.1016/j.mssp.2013.12.034.

[25] A. Okasha, M. B. Mohamed, S. Negm, and H. Talaat, "Weak exciton-plasmon and exciton-phonon coupling in chemically synthesized Ag/CdSe metal/semiconductor hybrid nanocomposite," Phys. E Low-Dimensional Syst. Nanostructures, vol. 44, no. 10, pp. 2094–2098, 2012, doi: 10.1016/j.physe.2012.06.022.

[26] F. Horia, K. Easawi, R. Khalil, S. Abdallah, M. El-Mansy, and S. Negm, "Optical and Thermophysical Characterization of Fe3O4 Nanoparticle," IOP Conf. Ser. Mater. Sci. Eng., vol. 956, no. 1, 2020, doi: 10.1088/1757-899X/956/1/012016.

[27] K. Easawi, M. Nabil, T. Abdallah, S. Negm, and H. Talaat, "Plasmonic Absorption Enhancement in Au/CdS Nanocomposite," World Acad. Sci. Eng. Technol., vol. 6, no. 61, pp. 63–66, 2012.